Modelling the growth of ZnO nanocombs based on the piezoelectric effect

F. Fattahi Comjani, U. Willer, S. Kontermann, and W. Schade

Citation: AIP Advances **3**, 102102 (2013); doi: 10.1063/1.4824616
View online: http://dx.doi.org/10.1063/1.4824616
View Table of Contents: http://scitation.aip.org/content/aip/journal/adva/3/10?ver=pdfcov
Published by the AIP Publishing

AIP ADVANCES **3**, 102102 (2013)

Modelling the growth of ZnO nanocombs based on the piezoelectric effect

F. Fattahi Comjani,[1,a] U. Willer,[1] S. Kontermann,[2] and W. Schade[1,2]
[1]*Institute of Energy Research and Physical Technologies, Clausthal University of Technology, Goslar, 38640, Germany*
[2]*Fraunhofer Heinrich-Hertz-Institute, Goslar, 38640, Germany*

(Received 21 July 2013; accepted 25 September 2013; published online 2 October 2013)

In this work a model for the growth of ZnO nanocombs based on the piezoelectric character of ZnO is presented that explains the periodic growth of nanowire branches on the polar +(0001) surface of a ZnO nanobelt as a self catalytic growth process. In this model the perturbation and elasticity theory are applied to approximate the induced mechanical strain and piezoelectric potential distribution in the nanobelt under the growth kinetics. To implement a quantitative simulation of the periodic growth of ZnO nanobranches the induced piezoelectric charges in the ZnO nanostructure are calculated. These are responsible for the structural transformation from a nanobelt into a nanocomb. A comparison with nanocombs that are synthesized using the vapor-liquid-solid method shows good agreement between experimental and theoretical results. [http://dx.doi.org/10.1063/1.4824616]

I. INTRODUCTION

ZnO with abundant configurations of nanostructures such as nanowires,[1–3] nanaohelices,[4,5] nanobelts,[4–6] nanoplates,[7] nanobridges,[8] nanonails,[8] nanosails,[9] and nanocombs,[10–13] is one of the most important functional semiconductor nanomaterials. Due to its wide direct band gap of 3.37 eV and a large exciton binding energy of 60 meV,[14] ZnO, especially aligned ZnO nanowires have applications in optoelectronic devices,[15,16] and sensors.[17–20] Its unique semiconducting and piezoelectric properties[21,22] in combination with high mechanical strength make ZnO nanostructures suitable for the application in nanoresonators[23] and nanogenerators.[24–27] Recently, ZnO comb-like nanostructures, in which nanowire branches are distributed in an ordered manner on one or both sides of the backbone nanobelt, have attracted considerable attention for the application to nanocantilevers,[28] UV nanolaser arrays,[29] optical nanogratings,[11,30] nanopolarizer,[11] and biosensors.[31] ZnO nanocomb structures can be synthesized by a carbothermal reduction process between graphite carbon and ZnO powder at temperatures higher than 900 °C.[10,11,27–32] In this process a high Zn vapor pressure is essential. In previous studies mechanisms for the growth of ZnO nanocombs have been proposed, which relate the formation of nanocombs with the self catalytic effect possibly due to the Zn cluster at the defective site on the polar +(0001) surface of the ZnO nanobelt[10] or the enrichment of Zn at the growth front +(0001).[28] However, these mechanisms cannot explain the growth of parallel and evenly spaced nanowire branches of a nanocomb on the polar +(0001) surface of the backbone nanobelt, which may be important to control the growth process of nanocombs and consequently to develop the nanoscale functional devices based on them.

In this work, we apply the perturbation and elasticity theory to approximate the induced strain distribution in the ZnO nanobelt under the growth kinetics and explain how the coupling of the mechanical strain to the piezoelectric field across the nanobelt thickness leads to periodic vertical

[a]Electronic mail: f.fattahi@pe.tu-clausthal.de.

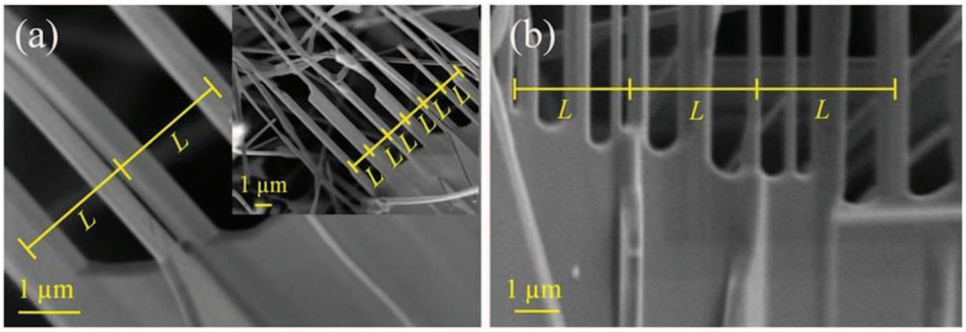

FIG. 1. SEM images of two ZnO nanocombs synthesized on Si (111) substrate by VLS method. L is the periodicity of the nanowire branches grown on the backbone nanobelt. The ZnO nanocombs in (a) and (b) have a different geometry: (a) $\bar{L} = 2.10\ \mu$m and (b) $\bar{L} = 2.76\ \mu$m. Reproduced with permission from ref. 33. Copyright Wiley-VCH Verlag GmbH & Co. KGaA, 2013.

displacements along the nanobelt length, which are the preferred places for the self catalytic growth of the nanowire branches for building a nanocomb structure. Drawing on the example of a real structure the ZnO nanocomb (Fig. 1(b)) synthesized by the vapor-liquid-solid (VLS) method is modelled.[33]

ZnO crystals grow anisotropically due to the different surface energies of different crystal faces.[34–37] The calculated values for surface cleavage energy for the +(0001), −(0001), (11–20) and (10–10) surfaces are 4.3, 4.3, 2.5 and 2.3 J/m^2 respectively.[34] This suggests that the polar ±(0001) surfaces are the least stable faces of ZnO. That is why most commonly the ZnO nanostructures grow fastest in direction [0001] and have only small polar ±(0001) surfaces. However one can overcome the barrier of surface energy by controlling the growth kinetics and achieve (0001) surface-dominated nanostructures e.g. nanobelts and nanocombs.[4,5] The ZnO nanocombs shown in Fig. 1 were grown by the VLS method in a horizontal three-zone furnace (with Ar as carrier gas) on a Si (111) substrate. The substrate was coated with 2.5 nm Au as catalyst. The synthesis of these structures are described in detail elsewhere.[33] The synthesized ZnO nanocombs (Figs. 1(a) and 1(b)) have different geometrical shapes. Our approach to explain the periodic geometrical shape of the ZnO nanocombs is given below.

II. THEORETICAL SOLUTIONS

A. The perturbation theory

A static piezoelectric system can be completely described with the Gauss equation for the electric field, the mechanical equilibrium equation, the constitutive equation and the compatibility equation along with appropriate boundary conditions.[38,39] In order to simplify the analytical solution of these equations, one can apply the perturbation expansion of the linear equations introduced by Wang and Gao:[40] The different orders of electromechanical coupled effect are achieved by introducing a perturbation parameter in the constitutive equations. The first two orders of these perturbation equations are given as follows:[40]

$$\sigma_p^{(0)} = c_{pq}\varepsilon_q^{(0)}, \tag{1}$$

$$D_i^{(0)} = k_{ik}E_k^{(0)}, \tag{2}$$

$$\sigma_p^{(1)} = c_{pq}\varepsilon_q^{(1)} - e_{kp}^T E_k^{(0)}, \tag{3}$$

$$D_i^{(1)} = e_{iq}\varepsilon_q^{(0)} + k_{ik}E_k^{(1)}, \tag{4}$$

where σ is the stress tensor, ε is the strain tensor, E is the electric field vector and D is the electric displacement vector, which are related for the first two order as above. Here c_{pq} is the linear elastic constant, e_{kp} is the linear piezoelectric coefficient, ${e^T}_{kp}$ is the transpose of the element e_{kp} and k_{ik} is the dielectric constant of the material. For a ZnO crystal with the C_{6v} symmetry, c_{pq}, e_{kp}, and k_{ik} can be written as

$$c_{pq} = \begin{pmatrix} c_{11} & c_{12} & c_{13} & 0 & 0 & 0 \\ c_{12} & c_{11} & c_{13} & 0 & 0 & 0 \\ c_{13} & c_{13} & c_{33} & 0 & 0 & 0 \\ 0 & 0 & 0 & c_{44} & 0 & 0 \\ 0 & 0 & 0 & 0 & c_{44} & 0 \\ 0 & 0 & 0 & 0 & 0 & \dfrac{(c_{11} - c_{12})}{2} \end{pmatrix}, \tag{5}$$

$$e_{kp} = \begin{pmatrix} 0 & 0 & 0 & 0 & e_{15} & 0 \\ 0 & 0 & 0 & e_{15} & 0 & 0 \\ e_{31} & e_{31} & e_{33} & 0 & 0 & 0 \end{pmatrix}. \tag{6}$$

$$k_{ik} = \begin{pmatrix} k_{11} & 0 & 0 \\ 0 & k_{11} & 0 \\ 0 & 0 & k_{33} \end{pmatrix}. \tag{7}$$

In this work the solutions of the first two orders are considered for the case of a ZnO nanobelt. For ZnO nanocombs reported in previous studies, the preferred growth direction for the backbone nanobelts are either [01-10] with the side dominated surfaces being (2-1-10)[10,11,13,30] or [2-1-10] with the side dominated surfaces being (01–10).[28] However, for all of them the polar surfaces ±(0001) at the top and bottom end of the nanobelts, are terminated by Zn^{2+} and O^{2-} ions. These polar surfaces (spontaneous polarization) introduce an intrinsic electric field ${E_k}^{(0)}$ inside of the nanobelts. For the case of the thick nanobelt shown in Fig. 1 (with the assumption of the polar surfaces ±(0001) at the top and bottom end of the nanobelt in reference to the previous studies), we ignore ${E_k}^{(0)}$ and its contribution to the coupling between mechanical field and electric field. Consequently one can take ${\sigma_p}^{(1)} = 0$, ${\varepsilon_q}^{(1)} = 0$ in Eq. (3). Thus in the free standing ZnO nanobelt, the first two orders of the perturbation equations become

$$\sigma_p^{(0)} = c_{pq}\varepsilon_q^{(0)}, \tag{8}$$

$$D_i^{(1)} = e_{iq}\varepsilon_q^{(0)} + k_{ik}E_k^{(1)}, \tag{9}$$

The zeroth order solution is a purely mechanical deformation depending on the growth kinetics and the first order solution is the result of the direct piezoelectric effect meaning that the mechanical deformation in the material induces an electric field in the nanobelt.

B. Theory of elasticity

Because of the small displacement (Because of the small displacement ($\varepsilon_z = \Delta h/2H \sim 3\%$) (see Fig. 2 for the definition of Δh and H) in the backbone nanobelt shown in Fig. 1(b), the infinitesimal strain theory is used. Mao *et al.*[41] have reported that for the ZnO nanobelt, which is grown along the [0001] direction and enclosed by the (01–10), the hardness along [0001] may be higher than that along [2-1-10]. But to simplify the analytical solution the ZnO nanobelt is approximated as an isotropic elastic material with Young's modulus E and Poisson ratio ν. The strain and stress relation

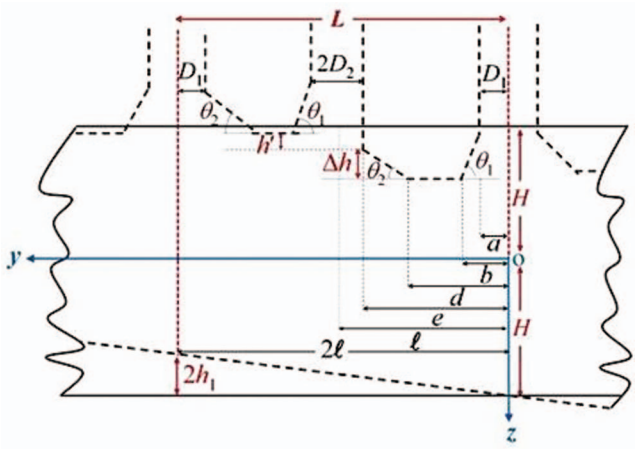

FIG. 2. Coordinate system and schematic geometry of the ZnO nanocomb in two dimensions. The black line shows the primary nanobelt with a thickness of $2H$ and the dashed line shows the final geometry of the nanocomb. L is the periodicity of the nanowire branches grown on the top polar +(0001) surface of the nanobelt.

(Hooke's law) is written as[40]

$$\begin{pmatrix} \varepsilon_x^{(1)} \\ \varepsilon_y^{(1)} \\ \varepsilon_z^{(1)} \\ \gamma_{yz}^{(1)} \\ \gamma_{zx}^{(1)} \\ \gamma_{xy}^{(1)} \end{pmatrix} = \frac{1}{E} \begin{pmatrix} 1 & -\nu & -\nu & 0 & 0 & 0 \\ -\nu & 1 & -\nu & 0 & 0 & 0 \\ -\nu & -\nu & 1 & 0 & 0 & 0 \\ 0 & 0 & 0 & 2(1+\nu) & 0 & 0 \\ 0 & 0 & 0 & 0 & 2(1+\nu) & 0 \\ 0 & 0 & 0 & 0 & 0 & 2(1+\nu) \end{pmatrix} \begin{pmatrix} \sigma_x^{(1)} \\ \sigma_y^{(1)} \\ \sigma_z^{(1)} \\ \tau_{yz}^{(1)} \\ \tau_{zx}^{(1)} \\ \tau_{xy}^{(1)} \end{pmatrix}, \tag{10}$$

where σ is the notation for the stress components acting perpendicular to the sides of the nanobelt parallel to Cartesian coordinate axes x, y, z (normal stress). τ is the notation for the stress components acting tangential to the sides of the nanobelt (shear stress). The first subscript letter for the shearing stress indicates the direction of the normal to the side under consideration and the second one indicates the direction of the stress component. Here ε is the notation for the components of the normal strain and γ is the notation for the components of the shear strain in the same manner.

To further simplify, we assume that the nanobelt has its edges parallel to two perpendicular axes of elastic symmetry with a uniform rectangular cross section. The coordinate axes y and z are chosen as shown in Fig. 2. Because of the small width of the nanobelt in comparison to its thickness (see Fig. 1) the problem can be treated as a case of the plane stress ($\sigma_x{}^{(0)} = 0$, $\tau_{zx}{}^{(0)} = \tau_{xy}{}^{(0)} = 0$). In the most general case the distribution of vertical loading along the upper and lower edges of a beam can be expressed as Fourier series

$$q_{upper}(y) = a_0 + \sum_{n=1}^{\infty} a_n \cos \alpha y + \sum_{n=1}^{\infty} a'_n \sin \alpha y, \tag{11}$$

$$q_{lower}(y) = b_0 + \sum_{n=1}^{\infty} b_n \cos \alpha y + \sum_{n=1}^{\infty} b'_n \sin \alpha y. \tag{12}$$

Here,

$$\begin{aligned}
&\alpha = n\pi/L,\\
&a_0 = (1/L)\int_0^L q_{upper}(y)\,dy,\\
&b_0 = (1/L)\int_0^L q_{lower}(y)\,dy,\\
&a_n = (2/L)\int_0^L q_{upper}(y)\cos\alpha y\,dy,\\
&a'_n = (2/L)\int_0^L q_{upper}(y)\sin\alpha y\,dy,\\
&b_n = (2/L)\int_0^L q_{lower}(y)\cos\alpha y\,dy,\\
&b'_n = (2/L)\int_0^L q_{lower}(y)\sin\alpha y\,dy.
\end{aligned} \tag{13}$$

The stress components are then obtained as follows:[38]

$$\begin{aligned}
\sigma_y = c_0 + \sum_{n=1}^{\infty} &\cos\alpha y[A_n\alpha^2\cosh\alpha z + B_n\alpha^2\sinh\alpha z\\
&+C_n\alpha(2\sinh\alpha z + \alpha z\cosh\alpha z) + D_n\alpha(2\cosh\alpha z + \alpha z\\
&\sinh\alpha z)] + \sum_{n=1}^{\infty}\sin\alpha y[A'_n\alpha^2\cosh\alpha z + B'_n\alpha^2\sinh\alpha z\\
&+C'_n\alpha(2\sinh\alpha z + \alpha z\cosh\alpha z) + D'_n\alpha(2\cosh\alpha z + \alpha z\sinh\alpha z)],
\end{aligned} \tag{14}$$

$$\begin{aligned}
\sigma_z = f_0 - \sum_{n=1}^{\infty} &\cos\alpha y(A_n\alpha^2\cosh\alpha z + B_n\alpha^2\sinh\alpha z\\
&+C_n\alpha^2 z\cosh\alpha z + D_n\alpha^2 z\sinh\alpha z) - \sum_{n=1}^{\infty}\sin\alpha y(A'_n\alpha^2\\
&\cosh\alpha z + B'_n\alpha^2\sinh\alpha z + C'_n\alpha^2 z\cosh\alpha z + D'_n\alpha^2 z\sinh\alpha z),
\end{aligned} \tag{15}$$

$$\begin{aligned}
\tau_{yz} = d_0 + \sum_{n=1}^{\infty} &\sin\alpha y[A_n\alpha^2\sinh\alpha z + B_n\alpha^2\cosh\alpha z\\
&+C_n\alpha(\cosh\alpha z + \alpha z\sinh\alpha z) + D_n\alpha(\sinh\alpha z + \alpha z\\
&\cosh\alpha z)] - \sum_{n=1}^{\infty}\cos\alpha y[A'_n\alpha^2\sinh\alpha z + B'_n\alpha^2\cosh\alpha z\\
&+C'_n\alpha(\cosh\alpha z + \alpha z\sinh\alpha z) + D'_n\alpha(\sinh\alpha z + \alpha z\cosh\alpha z)],
\end{aligned} \tag{16}$$

where the constants A_n, B_n, C_n, D_n, A'_n, B'_n, C'_n, and D'_n can be determined from the boundary conditions on the upper and lower edges of the nanobelt at $z = \pm H$. From the strain-displacement relationships and the Hooke's law, the following equations can be obtained:

$$\dot{E}V = \int(\sigma_y - \nu\sigma_z)\,dy + \dot{E}\,k_0\,z + k_1, \tag{17}$$

$$\dot{E}W = \int(\sigma_z - \nu\sigma_y)\,dz - \dot{E}\,k_0\,y + k_2, \tag{18}$$

$$\gamma_{yz} = \frac{\tau_{yz}}{G} = \frac{\partial V}{\partial z} + \frac{\partial W}{\partial y}, \tag{19}$$

$$G = \frac{\dot{E}}{2(1+\nu)}. \tag{20}$$

Here V and W are the displacement components parallel to the coordinate axes y and z, respectively. k_0, k_1 and k_2 are the constants, which are determined from the known displacements at the ends of the nanobelt. The constant G is called shear modulus or the modulus of rigidity.

C. Result of the electromechanical coupling in the ZnO nanobelt

By controlling the growth kinetics, ZnO comb-like nanostructures with a variety of periodicity and geometrical shapes, can be synthesized.[10,11,30] For each ZnO nanocomb the periodicity of its

TABLE I. The elastic and electric constants for bulk ZnO.[40] k_{11}, k_{22} and k_{33} are the dielectric constants of the material. e_{31}, e_{33} and e_{15} are the piezoelectric coefficients. E is Young's modulus and ν is Poisson ratio.

Constant	Value	Constant	Value
k_{11}	7.77	e_{31}	−0.51
k_{22}	7.77	e_{33}	1.22
k_{33}	8.91	e_{15}	−0.45
ν	0.349	E (GPa)	129

nanowire branches, the position of the facet at the nanowire-side (Lengths a and e in Fig. 2) and at the nanobelt-side (Lengths b and d in Fig. 2) determine the appropriate boundary conditions uniquely. Drawing on the example of a real structure the ZnO nanocomb shown in Fig. 1(b) is considered, which represents a more general deformation in the crystal structure of the primary nanobelt. In this case the boundary conditions are taken as follows:

$$\begin{aligned}
&V(0,z)=0, && V(2\ell,z)=constant,\\
&W(y,+H)=-\frac{h_1}{\ell}y, && W(2\ell,z)=-h_1,\\
&W(0,-H)=0, && W(\ell+d,-H)-W(e,-H)=-h',\\
&W(e,-H)-W(d,-H)=W(\ell+e,-H)-W(\ell+d,-H),\\
&W(a,-H)-W(b,-H)=W(\ell+a,-H)-W(\ell+b,-H),\\
&W(b,-H)-W(d,-H)=W(\ell+b,-H)-W(\ell+d,-H).
\end{aligned} \tag{21}$$

From these boundary conditions and equilibrium equations $\Sigma F_y = 0$, $\Sigma F_z = 0$ for the force components in y- and z-direction the constants constants A_n, B_n, C_n, D_n, A'_n, B'_n, C'_n, D'_n, c_0, f_0, d_0 in Eqs. (14)–(16) and the constants k_0, k_1, k_2 in Eqs. (17) and (18) are derived. Consequently by substituting Eqs. (14)–(16) into Eq. (10), the strain distribution in the nanobelt is determined. The values given in Table I for E and ν are used in our calculations. From the first two boundary conditions one find that n in the Fourier expansions (Eqs. (14)–(16)) must be an even number. With taking $n = 2$ the solution for the first three orders can be approximated. Using the Wolfram Mathematica 8.0, the strain distribution in the ZnO nanobelt is simulated as shown in Fig. 3. In the problem of plane stress ($\sigma_x^{(0)} \sim 0$) for the ZnO nanocomb a non zero strain $\varepsilon_x^{(0)}$ across the width of the nanobelt is to be calculated (Fig. 3(a)). This is caused by the normal stress components $\sigma_y^{(0)}$ and $\sigma_z^{(0)}$. The positive strain is corresponding to the induced tension and the negative strain to the induced compression in the nanobelt.

Now by using the perturbation approximation in Eq. (9) one obtains the induced piezoelectric field $E_k^{(1)}$ in the ZnO nanobelt. By noting that there is no free body charge in the nanobelt one takes

$$0 = \nabla \cdot e_{iq}\varepsilon_q^{(0)} + \nabla \cdot k_{ik}E_k^{(1)}, \tag{22}$$

in which

$$\nabla \cdot e_{iq}\varepsilon_q^{(0)} = \frac{\partial}{\partial y}e_{15}\gamma_{yz}^{(0)} + \frac{\partial}{\partial z}(e_{31}\varepsilon_x^{(0)} + e_{31}\varepsilon_y^{(0)} + e_{33}\varepsilon_z^{(0)}), \tag{23}$$

$$\nabla \cdot k_{ik}E_k^{(1)} = \frac{\partial}{\partial x}k_{11}E_x^{(1)} + \frac{\partial}{\partial y}k_{11}E_y^{(1)} + \frac{\partial}{\partial z}k_{33}E_z^{(1)}. \tag{24}$$

By using $E = -\nabla\varphi^{(1)}$ in Eq. (24) one obtains

$$\nabla \cdot k_{ik}E_k^{(1)} = -k_{11}\frac{\partial^2\varphi^{(1)}}{\partial x^2} - k_{11}\frac{\partial^2\varphi^{(1)}}{\partial y^2} - k_{33}\frac{\partial^2\varphi^{(1)}}{\partial z^2}. \tag{25}$$

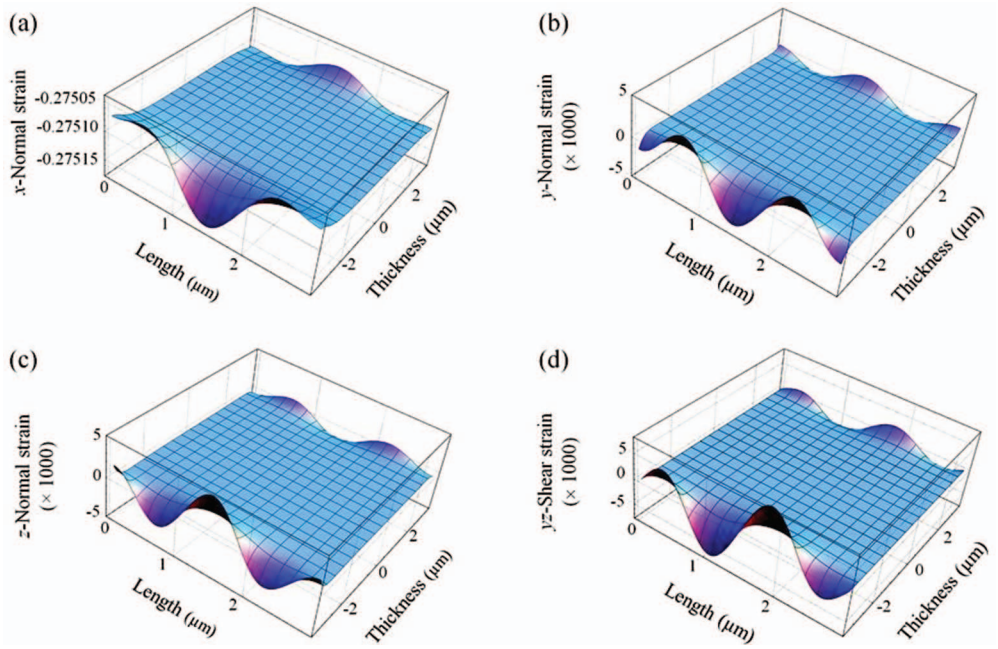

FIG. 3. Induced strain in the primary nanobelt for the ZnO nanocomb shown in Fig. 1(b). The components of the normal strain in (a) *x*-, (b) *y*-, (c) *z*-direction and (d) the shear strain in the nanobelt.

Since the $\nabla \cdot e_{iq}\ \varepsilon_q^{(0)}$ is independent of x, the induced piezoelectric potential $\varphi^{(1)}$ is uniform in x direction. In addition, because of the Fourier series expansion of $\nabla \cdot e_{iq}\ \varepsilon_q^{(0)}$, one can take $\varphi^{(1)}$ as a Fourier series expansion, which satisfies the Maxwell's law $\nabla \times E^{(1)} = 0$ too:

$$\varphi^{(1)} = \sum_{n=1}^{\infty} S_n(\mathrm{z})\ \sin\ \alpha y + \sum_{n=1}^{\infty} T_n(\mathrm{z})\ \cos\ \alpha y. \tag{26}$$

Here $S_n(z)$ and $T_n(z)$ are functions of z. By substituting Eq. (26) into Eq. (25) and solving Eq. (22) for the electric potential inside the nanobelt and the Laplace equation for the electric potential outside the nanobelt one obtains the induced piezoelectric potential and consequently the piezoelectric field in the nanobelt (Figs. 4(a) and 4(b)). The values given in Table I for the constants e_{kp} and k_{ik} are used in this calculation.

Figures 3(a)–3(d) and Fig. 4(a) show that the induced strain and electric potential within the nanobelt are noticeable only in the first layers under the top and bottom surfaces. A comparison between the induced electric potential distribution (Fig. 4(a)) and the normal strain distribution in *z*-direction in the nanobelt (Fig. 3(c)) indicates that positive and negative electric potentials are generated in the regions stretched and compressed along the polar axis of the nanobelt, respectively. The induced piezoelectric field distribution in the ZnO nanobelt is consistent with the mechanical deflection distribution in the material. This is shown for example in Figs. 4(b) and 4(c) only for the first layers under the top polar +(0001) surface of the nanobelt.

The red lines in Fig. 4(c) show schematically the expected geometry of the final nanostructure, which does not match exactly the geometry of the nanocomb shown in Fig. 2. This is because of the fact that in our calculations only the first three orders in the Fourier expansions (Eqs. (14)–(16)) are taken into account. To obtain a more precise solution one needs to consider higher orders in the Fourier expansions. Thus more boundary conditions are required. This may be achieved by using the transmission electron microscopy (TEM) images of a nanocomb, illustrating more details about the facets at the nanowire-side and at the nanobelt-side.

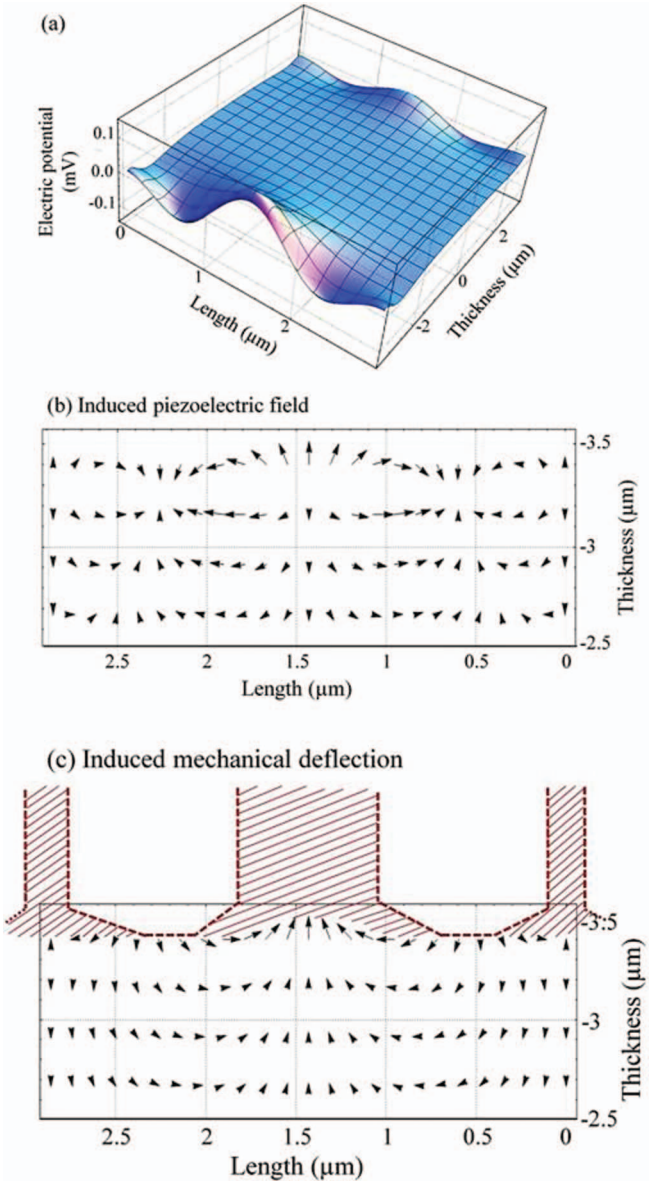

FIG. 4. (a) Induced piezoelectric potential distribution in the primary nanobelt. (b) corresponding piezoelectric field distribution and (c) mechanical deflection in the first layers under the top polar +(0001) surface of the nanobelt at $z = -H$ (see Fig. 2). The red lines show the schematic geometry of the final ZnO nanocomb.

III. MODEL OF GROWTH

ZnO crystallizes in the wurtzite structure without a center of inversion (Fig. 5(a)). That means by cleaving the crystal perpendicular to the *c* axis, two polar surfaces on opposite sides of the crystal are formed. The polar +(0001) surface has only Zn^{2+} ions and the polar –(0001) surface has only O^{2-} ions. Such a system may be considered as a "slab" of Zn-O double layers,[21,34] as shown in Fig. 5(b).

The $\nabla \cdot e_{iq}\ \varepsilon_q^{(0)}$ in Eq. (22) can be considered as a body charge density and it means that actually the divergence of the strain $\varepsilon_q^{(0)}$ in the material induces a piezoelectric field $E_k^{(1)}$ in the nanostructure. We call this body charge density, induced piezoelectric charge density. As shown in Fig. 6(a) the induced piezoelectric charge is localized in the surface regions and decays to zero in the middle of the nanobelt. A comparison between the induced piezoelectric charge and deflection

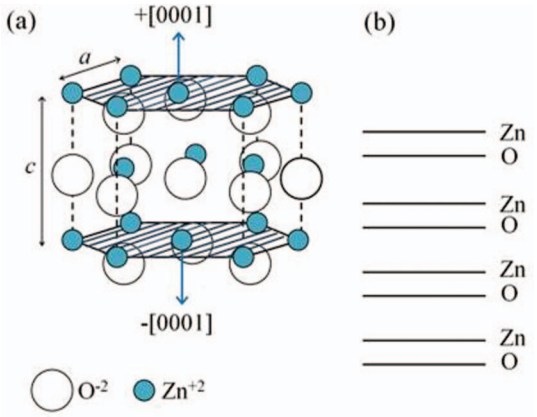

FIG. 5. Crystal structure of ZnO. (a) Wurtzite structure of ZnO with the top polar Zn-terminated +(0001) surface and the bottom polar O-terminated –(0001) surface. a and c are the crystal parameters of ZnO. (b) Schematic illustration of Zn-O double layers in a slab of the material.

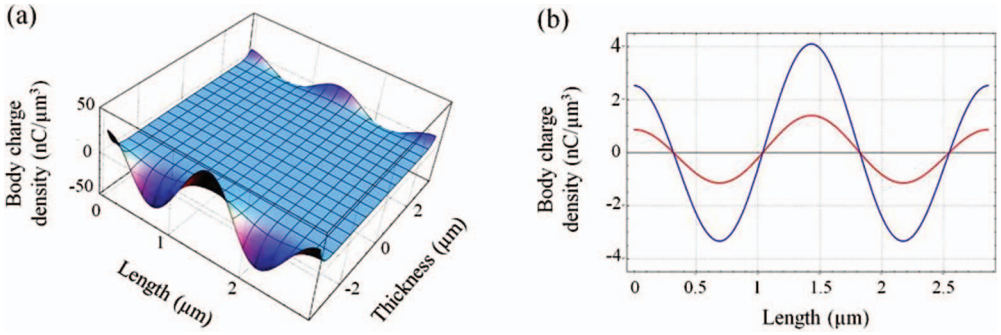

FIG. 6. Induced piezoelectric body charge density (a) in the nanobelt (b) in the top surface layer at $z = -H$ (blue line) and in the bottom surface layer at $z = +H$ (red line).

distribution suggests a rearrangement of charges between the first Zn-O double layers under the top and bottom polar surfaces of the nanobelt. In the stretched regions of the nanobelt, the Zn-terminated side gets farther away from the O-terminated side and becomes more positively charged. On the other hand, in the compressed regions the Zn-terminated side gets closer to the O-terminated side and becomes less positively charged. It follows that the top polar +(0001) surface (at $z = -H$) of the nanobelt has no homogenous Zn^{2+} ion density (see Fig. 6(b)).This suggests a self catalytic growth of ZnO nanowire branches on the polar +(0001) surface at the regions with higher positive charge density and hence more metal content compared to its vicinity. Therefore the nanowire branches grow periodically on the top polar surface and thus the nanobelt changes into a nanocomb. Similarly, on the bottom polar –(0001) surface (at $z = +H$), the O^{2-} ion density is not homogenous too (see Fig. 6(b)) but this causes no metallic catalyst for the growth of ZnO nanowire branches. Hence the nanowire branches grow only on the top polar +(0001) surface of the nanobelt.

As mentioned already, the periodicity of the nanowire branches on the nanobelt depends on the growth kinetic control. In our experiment the Ar flow fluctuation, relatively low zinc vapor pressure and temperature fluctuation in the growth process may cause different periodicities of the nanowire branches of the same nanocomb as well their irregular length and width as shown in Fig. 1.

IV. CONCLUSIONS

In summary, we presented a model for the growth of ZnO nanocomb structures based on the piezoelectric character of ZnO. Applying the perturbation and elasticity theory and using the Fourier expansion of mechanical stress exerted in the material under the growth kinetics, the induced

piezoelectric charge in the nanostructure is approximated. The periodic distribution of the induced piezoelectric charge explains the periodic growth of nanowire branches of ZnO nanocombs on the polar +(0001) surface as a consequence of a self catalytic growth process.

ACKNOWLEDGMENTS

We acknowledge support by Open Access Publishing Fund of Clausthal University of Technology.

[1] M. H. Huang, Y. Wu, H. Feick, N. Tran, E. Weber, and P. Yang, Adv. Mater. **13**, 113 (2001).
[2] S. Y. Li, P. Lin, C. Y. Lee, and T. Y. Tseng, J. Appl. Phys. **95**, 3711 (2004).
[3] A. Kushwaha, H. Tyagi, and M. Aslam, AIP ADVANCES **3**, 042110 (2013).
[4] X. Y. Kong and Z. L. Wang, Nano Lett. **3**, 1625 (2003).
[5] P. X. Gao and Z. L. Wang, J. Appl. Phys. **97**, 044304 (2005).
[6] X.-S. Fang, C.-H. Ye, L.-D. Zhang, Y. Li, and Z.-D. Xiao, Chem. Lett. **34**, 436 (2005).
[7] C. Ye, X. Fang, Y. Hao, X. Teng, and L. Zhang, J. Phys. Chem. B **109**, 19758 (2005).
[8] J. Y. Lao, J. Y. Huang, D. Z. Wang, and Z. F. Ren, Nano Lett. **3**, 235 (2003).
[9] S. Jebril, H. Kuhlmann, S. Müller, C. Ronning, L. Kienle, V. Duppel, Y. K. Mishra, and R. Adelung, Crystal Growth & Design **10**, 2842 (2010).
[10] Y. S. Lim, J. W. Park, S.-T. Hong, and J. Kim, Materials Science and Engineering B **129**, 100 (2006).
[11] K. Yu, Q. Zhang, J. Wu, L. Li, Y. Xu, S. Huang, and Z. Zhu, Nano Res. **1**, 221 (2008).
[12] C. H. Zang, Y. C. Liu, D. X. Zhao, J. Y. Zhang, and D. Z. Shen, J. Nanosci. Nanotechnol. **10**, 2370 (2010).
[13] T. Xu, P. Ji, M. He, and J. Li, J. Nanomater. 797935 (2012).
[14] X. Fang, Y. Bando, U. K. Gautam, C. Ye, and D. Golberg, J. Mater. Chem. **18**, 509 (2008).
[15] W. Y. Weng, S. J. Chang, C. L. Hsu, and T. J. Hsueh, ACS Appl. Mater. Interfaces **3**, 162 (2011).
[16] K. Wang, J. J. Chen, Z. M. Zeng, J. Tarr, W. L. Zhou, Y. Zhang, Y. F. Yan, C. S. Jiang, J. Pern, and A. Mascarenhas, Appl. Phys. Lett. **96**, 123105 (2010).
[17] D. Pradhan, F. Niroui, and K. T. Leung, ACS Appl. Mater. Interfaces **2**, 2409 (2010).
[18] M.-W. Ahn, K.-S. Park, J.-H. Heo, D.-W. Kim, K. J. Choi, and J.-G. Park, Sensors and Actuators B **138**, 168 (2009).
[19] S. M. Al-Hilli, R. T. Al-Mofarji, P. Klason, M. Willander, N. Gutman, and A. Sa'ar, J. Appl. Phys. **103**, 014302 (2008).
[20] X. Fang, L. Hu, C. Ye, and L. Zhang, Pure Appl. Chem. **82**, 2185 (2010).
[21] Ü. Özgür, Ya. I. Alivov, C. Liu, A. Teke, M. A. Reshchikov, S. Doğan, V. Avrutin, S.-J. Cho, and H. Morkoç, J. Appl. Phys. **98**, 041301 (2005).
[22] D. A. Scrymgeour, T. L. Sounart, N. C. Simmons, and J. W. Hsu, J. Appl. Phys. **101**, 014316 (2007).
[23] B. A. Buchine, W. L. Hughes, F. L. Degertekin, and Z. L. Wang, Nano Lett. **6**, 1155 (2006).
[24] Z. L. Wang and J. Song, Science **312**, 242 (2006).
[25] X. Wang, J. Song, J. Liu, and Z. L. Wang, Science **316**, 102 (2007).
[26] C. Periasamy and P. Chakrabarti, J. Appl. Phys. **109**, 054306 (2011).
[27] Y. Hu, Y. Zhang, C. Xu, G. Zhu, and Z. L. Wang, Nano Lett. **10**, 5025 (2010).
[28] Z. L. Wang, X. Y. Kong, and J. M. Zuo, Phys. Rev. Lett **91**, 185502 (2003).
[29] H. Yan, R. He, J. Johnson, M. Law, R. J. Saykally, and P. Yang, J. Am. Chem. Soc. **125**, 4728 (2003).
[30] Z. W. Pan, S. M. Mahurin, S. Dai, and D. H. Lowndes, Nano Lett. **5**, 723 (2005).
[31] J. X. Wang, X. W. Sun, A. Wei, Y. Lei, X. P. Cai, C. M. Li, and Z. L. Dong, Appl. Phys. Lett. **88**, 233106 (2006).
[32] S. Y. Li, C. Y. Lee, and T. Y. Tseng, Journal of Crystal Growth **247**, 357 (2003).
[33] F. Fattahi Comjani, U. Willer, S. Kontermann, and W. Schade, Phys. Status Solidi A, in press (2013).
[34] B. Meyer and D. Marx, Phys. Rev. B. **67**, 035403 (2003).
[35] O. Dulub, L. A. Boatner, and U. Diebold, Surface Science **519**, 201 (2002).
[36] O. Dulub, U. Diebold, and G. Kresse, Phys. Rev. Lett. **90**, 016102 (2003).
[37] K. M. Wong, S. M. Alay-e-Abbas, A. Shaukat, Y. Fang, and Y. Lei, J. Appl. Phys. **113**, 014304 (2013).
[38] S. P. Timoshenko and J. N. Goodier, *Theory of Elasticity* (McGraw-Hill Book Co., New York, 1970) p. 46–49.
[39] T. Ikeda, *Fundamentals of Piezoelectricity* (Oxford University Press, New York, 1990) p. 16.
[40] Y. Gao and Z. L. Wang, Nano Lett. **7**, 2499 (2007).
[41] S. X. Mao and M. Zhao, Appl. Phys. Lett. **83**, 993 (2003).